Theory study on a photonic-assisted radio frequency phase shifter with direct current voltage control*

Li Jing(李 晶)[a)b)], Ning Ti-Gang(宁提纲)[a)b)], Pei Li(裴 丽)[a)b)†],
Jian Wei(简 伟)[a)b)], You Hai-Dong(油海东)[a)b)c)], Wen Xiao-Dong(温晓东)[a)b)],
Chen Hong-Yao(陈宏尧)[a)b)], Zhang Chan(张 婵)[a)b)], and Zheng Jing-Jing(郑晶晶)[a)b)]

[a)] *Key Laboratory of All Optical Network & Advanced Telecommunication Network of EMC, Beijing Jiaotong University, Beijing* 100044, *China*
[b)] *Institute of Lightwave Technology, Beijing Jiaotong University, Beijing* 100044, *China*
[c)] *Science and Information College, Qingdao Agricultural University, Qingdao* 266109, *China*

(Received 11 December 2013; revised manuscript received 4 April 2014; published online 10 August 2014)

A photonic-assisted radio frequency phase shifter with direct current voltage control is proposed using a polymer-based integrated Mach–Zehnder modulator. A closed-form expression of radio frequency (RF) signal power and phase is given. Theoretical calculation reveals that by carefully setting the bias voltages, RF signal power variation lower than 1-dB and phase accuracy less than 3° can be achieved and are not degraded by perturbation of modulation index once the bias voltage drift is kept within $-3\% \sim 3\%$.

Keywords: RF photonics, RF phase shifter, integrated Mach–Zehnder modulator

PACS: 42.79.Sz, 84.40.–x, 42.79.Hp **DOI:** 10.1088/1674-1056/23/10/104216

1. Introduction

Photonic radio frequency (RF) phase shifters have attracted considerable attention over the past few years in the area of microwave photonics.[1,2] They have quite a few advantages over traditional ones,[3,4] such as flexible tunability, high stability, and bandwidth, low cost and power consumption, and light weight offered by optical systems. With direct current (DC) voltage control, photonic phase shifters can be used to control multiple RF phases and feed the frequency-independent phase outputs into an phased array antenna to perform rapid and continuous beam-forming functions.[5,6] For all phase shifters, the following four characteristics should be met:[7,8] 1) a phase accuracy of 3° to satisfy most applications; 2) a phase control range of modulo-2π; 3) the ability to set the phase of an RF signal without altering its magnitude; and 4) low cost to enable individual element phase control. Various approaches to obtain photonic phase shifters have been reported. For instance, RF phase shifters can be realized using wavelength conversion in a distributed feedback (DFB) laser,[9] stimulated Brillouin scattering (SBS) signal processing,[10] homodyne mixing,[11] silicon microring resonator,[12] and semiconductor optical amplifier (SOA).[13,14] In addition to the above approaches, RF phase shifters can be also achieved by using electrical–optic modulators.[7,8,15] Generally, these modulators are fabricated in lithium niobate, GaAs, or InP. However, such a design suffers from high optical loss (roughly 5 dB) and limited operational bandwidth (around 40 GHz). Polymers are emerging as new and interesting materials for optical devices,[16,17] and these optical waveguides have attracted considerable attention for their inherent compactness, straightforward and simple fabrication, low optical loss, high-thermal stability, and most importantly high operational bandwidth, which can be extended to 110 GHz.[18]

In Ref. [5], a polymer-based RF phase shifter was proposed, which is composed of three phase modulation arms. The upper two arms are modulated with RF signal, and the third arm is driven by DC voltage. By setting a modulation index to 2.71, the phase shifter can be operated under linear phase shifting with no power variation. Then in Ref. [6], a single-chip integrated electro–optic polymer photonic RF phase shifter array with four phase modulation arms was proposed, in which two upper arms are single-sideband (SSB) modulated with RF signals, leaving the other two driven with DC voltage. It was shown that a highly linear RF phase over 360° with negligible RF power fluctuation can be achieved. However, the above two phase shifters share the same technical limit: the performance is dependent on the modulation index. For example, in Ref. [5] a desired performance can only be realized by setting the modulation index to 2.71, and in Ref. [6] the modulation should be carefully set according to the optical power-splitting ratio at the balancing arm. In other words, any perturbation of modulation index will degrade the performance, such as the RF signal power variation and phase accuracy.

In this work, using the same technology as in Refs. [5] and [6] we propose an RF phase shifter with direct current

*Project supported by the Fundamental Research Funds for the Central Universities of China (Grant No. 2014JBM013).
†Corresponding author. E-mail: lipei@bjtu.edu.cn
© 2014 Chinese Physical Society and IOP Publishing Ltd

voltage control as in Refs. [5] and [6]. The proposed RF phase shifter consists of two multimode interference (MMI) couplers (a 1×2 MMI and a 1×4 MMI), five pieces of phase modulation arms, and two optical combiners (OC) (a 4×1 OC and a 2×1 OC). A theoretical analysis is given with a closed-form expression of RF signal power and phase. Then a calculation is carried out to investigate the proposed technique. It is found that by carefully setting the bias voltage, phase shifting with an RF power variation lower than 1-dB and phase accuracy less than 3° can be realized. More importantly, the RF signal power and phase shifting are not dependent on the modulation index. The impact of bias voltage drift is also discussed and it is shown that the linear phase shifting can be obtained and is robust to modulation index if bias voltage drift is within −3%∼3%.

The paper is organized as follows. In Section 2, a theoretical analysis is given and a closed-form expression of the RF signal in power and phase is provided. In Section 3, discussion of performance in terms of RF signal power variation and phase accuracy is presented. In Section 4, we conclude this work.

2. Model and theory

Our proposed photonic-assisted RF phase shifter is shown in Fig. 1(a).

The input lightwave comes from a continuing wave laser described by the optical field of

$$E_{\text{in}}(t) = E_0 \exp(\text{j}\omega_0 t), \tag{1}$$

where E_0 denotes the magnitude of the optical field and ω_0 represents the angular frequency of optical carrier.

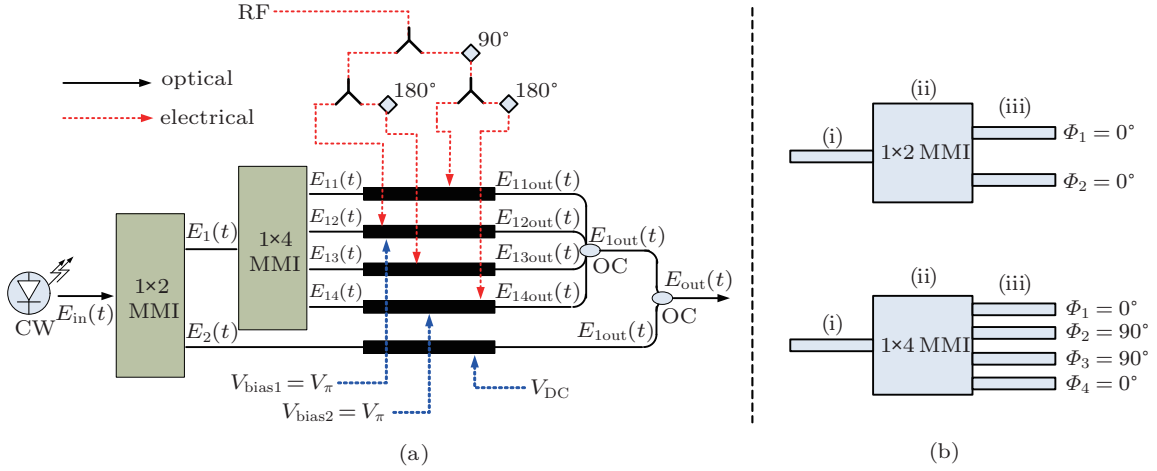


Fig. 1. (color online) (a) Setup of the proposed photonic RF phase shifter with dc voltage control; (b) Diagram of 1×2 MMI and 1×4 MMI coupler (CW: continue wave; MMI: multimode interference; OC: optical combiner).

Figure 1(a) shows the architecture of the polymer-based integrated Mach–Zehnder modulator (IMZM), which includes two multimode interference (MMI) couplers (a 1×2 MMI and a 1×4 MMI), five pieces of phase modulation arms, and two optical combiners (OC) (a 4×1 OC and a 2×1 OC). The MMI structure is based on self-imaging effects in multimode interference structures.[19] The operation principle of the proposed IMZM is similar to that of traditional optical–electrical modulators in Refs. [20] and [21]. Figure 1(b) is the diagram of 1×2 MMI and 1×4 MMI couplers. A typical MMI consists of a group of monomode waveguides (i) which define the input field, the wide multimode section (ii) where the interference effects of modal field occur, and the output monomode waveguide (iii). The 1×2 MMI coupler is similar to the 50:50 optical coupler, splitting the input optical field into two parts with equal intensities and phases $\Phi_1 = \Phi_2 = 0°$. The 1×4 MMI coupler splits the input optical field into four parts with equal intensities but different phases. The relative phase shifts of 1st, 2nd, 3rd, and 4th paths are $\Phi_1 = 0°$, $\Phi_2 = 90°$, $\Phi_3 = 90°$, and $\Phi_4 = 0°$ respectively.[16] The 1×2 MMI and 1×4 MMI can be described by the following equations

$$\begin{bmatrix} E_1(t) \\ E_2(t) \end{bmatrix} = \frac{1}{\sqrt{2}} \begin{bmatrix} \exp(\text{j}0) \\ \exp(\text{j}0) \end{bmatrix} E_{\text{in}}(t) \tag{2}$$

and

$$\begin{bmatrix} E_{11}(t) \\ E_{12}(t) \\ E_{13}(t) \\ E_{13}(t) \end{bmatrix} = \frac{1}{\sqrt{4}} \begin{bmatrix} \exp(\text{j}0) \\ \exp(\text{j}\frac{\pi}{2}) \\ \exp(\text{j}\frac{\pi}{2}) \\ \exp(\text{j}0) \end{bmatrix} E_1(t)$$

$$= \frac{1}{\sqrt{8}} \begin{bmatrix} \exp(\text{j}0) \\ \exp(\text{j}\frac{\pi}{2}) \\ \exp(\text{j}\frac{\pi}{2}) \\ \exp(\text{j}0) \end{bmatrix} E_{in}(t), \tag{3}$$

where $E_1(t)$, $E_2(t)$, $E_{11}(t)$, $E_{12}(t)$, $E_{13}(t)$, and $E_{14}(t)$ represent

the optical field as shown in Fig. 1(a). The driving RF signal is first input to a 90 ° hybrid coupler and the two outputs are then connected to two individual 180° hybrid couplers. Finally, four outputs directly drive the upper four phase modulation arms according to Fig. 1(a). In theory, the 90° hybrid coupler is used to obtain single sideband modulation, and the 180° hybrid couplers is used to obtain push–pull operation. Suppose that the driving RF signal is $v_{\rm RF}(t) = V_{\rm RF}\cos\Omega t$, where $V_{\rm RF}$ and $\Omega = 2\pi f$ denote the magnitude and angular frequency of RF. Therefore, the output optical field of each branch can be expressed as

$$E_{11\rm out}(t) = \frac{1}{\sqrt{8}}E_{\rm in}(t)\sum_{n=-\infty}^{\infty}(-1)^n J_n(m)\exp(\mathrm{j}n\Omega t), \quad (4)$$

$$E_{12\rm out}(t) = \frac{1}{\sqrt{8}}E_{\rm in}(t)\sum_{n=-\infty}^{\infty}j^{n+1}J_n(m)\exp(\mathrm{j}n\Omega t+\mathrm{j}\varphi_1), \quad (5)$$

$$E_{13\rm out}(t) = \frac{1}{\sqrt{8}}E_{\rm in}(t)\sum_{n=-\infty}^{\infty}(-\mathrm{j})^n J_n(m)\exp(\mathrm{j}n\Omega t), \quad (6)$$

$$E_{14\rm out}(t) = \frac{1}{\sqrt{8}}E_{\rm in}(t)\sum_{n=-\infty}^{\infty}J_n(m)\exp(\mathrm{j}n\Omega t+\mathrm{j}\varphi_2), \quad (7)$$

and

$$E_{2\rm out}(t) = \frac{1}{\sqrt{2}}E_{\rm in}(t)\exp(\mathrm{j}\varphi_3), \quad (8)$$

where $m = \pi V_{\rm RF}/2V_\pi$ is the modulation index, $\varphi_1 = \pi V_{\rm bias1}/V_\pi$ and $\varphi_2 = \pi V_{\rm bias2}/V_\pi$ are the bias-induced phase shift for the second and fourth branches, and $\varphi_3 = \pi V_{\rm DC}/V_\pi$ is the DC bias voltage-induced phase shift for the fifth branch, V_π is the half wave switching voltage to have π phase shift. For simplicity, power combining ratio of OC is assumed to be identical with the power splitting ratio of MMI. Then the optical field after the 2×1 OC becomes

$$\begin{aligned}E_{\rm out}(t) = \frac{1}{8}E_0\Bigg\{\sum_{n=-\infty}^{\infty}\Bigg[&\exp(\mathrm{j}\omega_0 t+\mathrm{j}n\Omega t+\mathrm{j}n\pi)\\&+\exp\left(\mathrm{j}\omega_0 t+\mathrm{j}n\Omega t+\mathrm{j}\frac{n+1}{2}\pi+\mathrm{j}\varphi_1\right)\\&+\exp\left(\mathrm{j}\omega_0 t+\mathrm{j}n\Omega t+\mathrm{j}\frac{3n+1}{2}\pi\right)\\&+\exp(\mathrm{j}\omega_0 t+\mathrm{j}n\Omega t+\mathrm{j}\varphi_2)\Bigg]J_n(m)\\&+4\exp(\mathrm{j}\omega_0 t+\mathrm{j}\varphi_3)\Bigg\}. \quad (9)\end{aligned}$$

In our case, small signal modulation is applied ($0 < m < \pi$), which means optical sidebands with order higher than 5th can be neglected without causing significant error. Then the optical intensity at the RF modulation frequency Ω can be concluded as

$$I_\Omega(t) \propto |\,E_{\rm out}(t)\,|^2 = A\cos\Omega t - B\sin\Omega t, \quad (10)$$

where A and B stand for the expression in Eq. (11) and Eq. (12):

$$\begin{aligned}A = \frac{E_0^2}{64}\Bigg\{&\sum_{n=-5}^{4}2J_n(m)J_{n+1}(m)\\&\times\Bigg[\sqrt{2}\sin\left(\frac{\varphi_2-\varphi_1}{2}\right)\sin\left(\frac{n}{2}\pi+\frac{3}{4}\pi+\frac{\varphi_1-\varphi_2}{2}\right)\\&+\sin(n\pi-\varphi_1)\\&-\sqrt{2}\sin\left(n\pi-\frac{\varphi_1+\varphi_2}{2}\right)\cos\left(\frac{n}{2}\pi-\frac{1}{4}\pi-\frac{\varphi_1-\varphi_2}{2}\right)\Bigg]\\&+8J_1(m)[2\cos(\varphi_3)-2\cos(\varphi_3-\varphi_1)]\Bigg\} \quad (11)\end{aligned}$$

and

$$\begin{aligned}B = \frac{E_0^2}{64}\Bigg\{&\sum_{n=-5}^{4}2J_n(m)J_{n+1}(m)\\&\times\Bigg[\sqrt{2}\sin\left(\frac{\varphi_2-\varphi_1}{2}\right)\sin\left(\frac{n}{2}\pi+\frac{3}{4}\pi+\frac{\varphi_1-\varphi_2}{2}\right)\\&-\sin(n\pi-\varphi_2)\\&+\sqrt{2}\sin\left(n\pi-\frac{\varphi_1+\varphi_2}{2}\right)\cos\left(\frac{n}{2}\pi-\frac{1}{4}\pi-\frac{\varphi_1-\varphi_2}{2}\right)\Bigg]\\&+8J_1(m)[2\sin(\varphi_3)-2\sin(\varphi_3-\varphi_2)]\Bigg\}. \quad (12)\end{aligned}$$

After optical to electrical conversion, the calculated RF signal power and phase at the RF modulation frequency can be obtained by

$$P_\Omega = A^2 + B^2 \quad (13)$$

and

$$\varphi_\Omega = \tan^{-1}\left(\frac{B}{A}\right). \quad (14)$$

In order to simplify the above theory and clearly show the approach of RF phase shifting, the bias voltage ($V_{\rm bias1}$ and $V_{\rm bias2}$ in Fig. 1(a)) is set as $V_{\rm bias1} = V_{\rm bias2} = V_\pi$. In that case, bias-induced phase shifts, i.e., $\varphi_1 = \varphi_2 = \pi$ in Eq. (11) and Eq. (12) can be obtained and the calculated RF signal power in Eq. (13) and phase in Eq. (14) can be simplified to

$$\begin{aligned}P_\Omega &= \frac{1}{4}E_0^4 J_1^2(m)[(\cos\varphi_3)^2+(\sin\varphi_3)^2]\\&= \frac{1}{4}E_0^4 J_1^2(m), \quad (15)\end{aligned}$$

$$\varphi_\Omega = \tan^{-1}\left[\frac{\frac{1}{2}E_0^2 J_1(m)\sin\varphi_3}{\frac{1}{2}E_0^2 J_1(m)\cos\varphi_3}\right] = \varphi_3 = \frac{\pi}{V_\pi}V_{\rm DC}. \quad (16)$$

Note that once the modulation index m is fixed, the RF power does not vary at all and the RF phase shift is highly linear with respect to the DC voltage $V_{\rm DC}$. Precise RF phase shifting without power variation can thus be achieved, which makes this approach an excellent solution to phase-array beam-forming and smart antenna systems.

3. Calculation and discussion

In practice, the proposed RF phase shifter may suffer from RF power variation and inaccurate phase shifting induced by two primary causes: One is due to the bias drift $\Delta V_{\text{bias}} = (\Delta V / V\pi) \times 100\%$ and the other is due to the perturbation of modulation index $\Delta m = (\Delta V_{\text{RF}}/2V\pi) \times 100\%$, where ΔV and ΔV_{RF} denote bias voltage drift and RF voltage drift respectively. Therefore, the bias-induced phase shift becomes $\varphi = \pi \times (1 + \Delta V_{\text{bias}})$. In our case, there are two bias-induced phase shift, i.e., $\varphi_1 = \pi \times (1 + \Delta V_1/V\pi)$ and

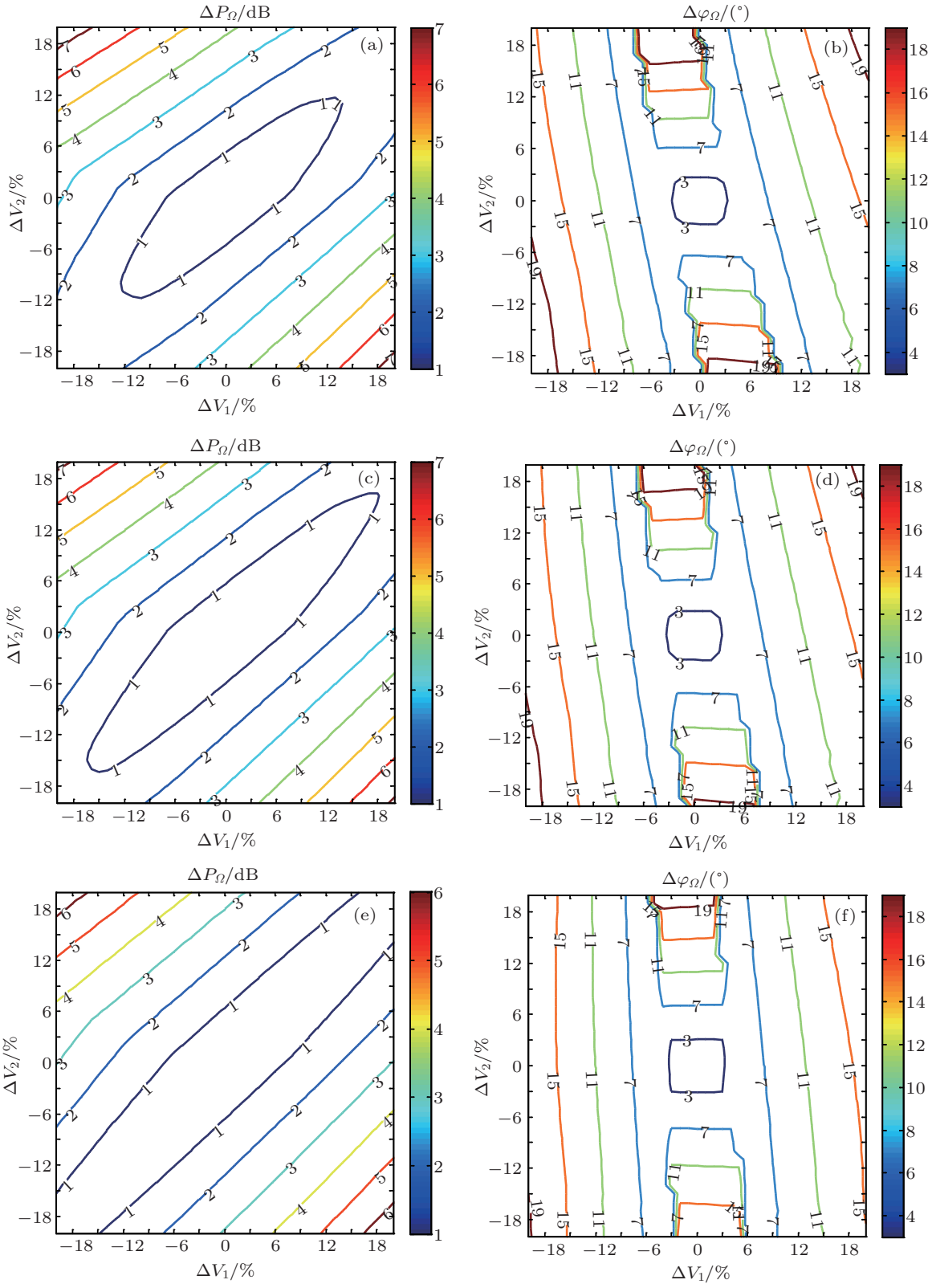


Fig. 2. (color online) Calculated RF power variation ΔP_Ω contour map at (a) $m = 0.5$, (c) $m = 1$, and (e) $m = 1.5$, and phase accuracy ΔP_Ω map at (b) $m = 0.5$, (d) $m = 1$, and (f) $m = 1.5$.

$\varphi_1 = \pi \times (1 + \Delta V_2 / V\pi)$. In this section, we will focus on RF signal power variation (in dB) and phase accuracy (in degree), which are defined in Eq. (17) and Eq. (18).

$$\Delta P_\Omega = 10\log_{10}[\max(A^2 + B^2)] - \log_{10}[\min(A^2 + B^2)] \quad (17)$$

and

$$\Delta\varphi_\Omega = \frac{180}{\pi} \max\left(\left|\tan^{-1}\left(\frac{B}{A}\right) - \varphi_3\right|\right), \quad (18)$$

where max and min denote the maximum and minimum values obtained within DC voltage's tunable range, $0 < V_{\rm DC} < 2V\pi$, corresponding to the phase shifting, $0 < \varphi_3 < 360^\circ$.

To quantify the impact of bias drift on ΔP_Ω in Eq. (17) and $\Delta\varphi_\Omega$ in Eq. (18), the perturbation of modulation index Δm is neglected first. Figure 2 shows the contour maps in (ΔV_1, ΔV_2), in which figures 2(a), 2(b), and 2(c) illustrate the RF signal power variations at modulation index of $m = 0.5$, $m = 1$, and $m = 1.5$ respectively. The RF power variation lower than 1 -dB can be clearly observed (a circle marked with 1 dB) in the center of the maps. With m increasing form 0.5 to 1.5, the impact of bias drift becomes smaller and smaller, which can be revealed by the range of 1-dB circle as shown in Figs. 2(a), 2(c), and 2(e). In other words, stable ΔP_Ω can be obtained at high modulation index. Then figures 2(b), 2(d), and 2(f) show the phase accuracy $\Delta\varphi_\Omega$ as a contour map of (ΔV_1, ΔV_2) at modulation index of $m = 0.5$, $m = 1$, and $m = 1.5$ respectively. Unlike the impact on ΔP_Ω, there is not much difference between these three maps. By observing the maps, we note that if $\Delta V_{\rm bias}$ is kept within the range of $-3\%\sim 3\%$, a phase accuracy less than 3° can be achieved. The same range also satisfies the requirement of RF signal power variation less than 1 dB in Figs. 2(a), 2(c), and 2(e). Therefore, biases drift range is supposed to be kept within $-3\%\sim 3\%$, such a range can be achieved by bias control circuit.

Now the perturbation of modulation index Δm is included. Without loss of generality, the bias drift considered is within the range of $-3\%\sim 3\%$. As a matter of fact, figure 2 has already illustrated that issue. It can be observed that both the RF signal power variation ΔP_Ω and phase accuracy $\Delta\varphi_\Omega$ do not change much with respect to different modulation index m. But, to clearly show the results, we consider four extreme bias cases in (ΔV_1, ΔV_2): case (a): (3%, 3%); case (b): (−3%, 3%); case (c): (−3% −3%); and case (d): (3%, −3%). Here, modulation index is set as $m = 1 + \Delta m$, where Δm varies from −50% to 50%. Figure 3 illustrates the evolution of ΔP_Ω and $\Delta\varphi_\Omega$ with Δm for the above four cases. As shown in Fig. 3, ΔP_Ω remains less than 1 dB and $\Delta\varphi_\Omega$ is less than around 3°. A good agreement with the results in Fig. 2 is predicted. Technically, the modulation index can be chosen randomly and any perturbation will not be a concern, which is an advantage of this work when compared to Refs. [5], and [6].

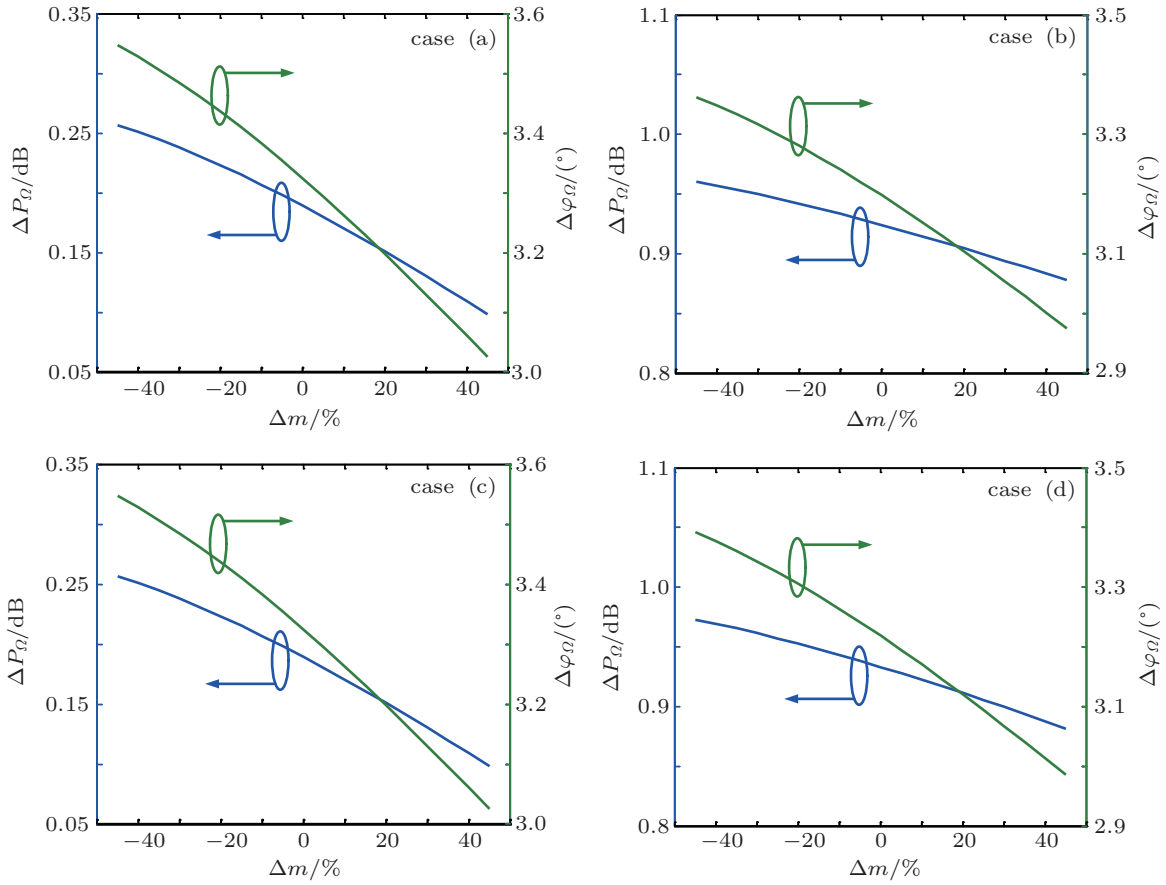


Fig. 3. (color online) Calculated RF power variation ΔP_Ω and phase accuracy $\Delta\varphi_\Omega$ with Δm for case (a): (3%, 3%); case (b): (−3%, 3%); case (c): (−3%, −3%); case (d): (3%, −3%).

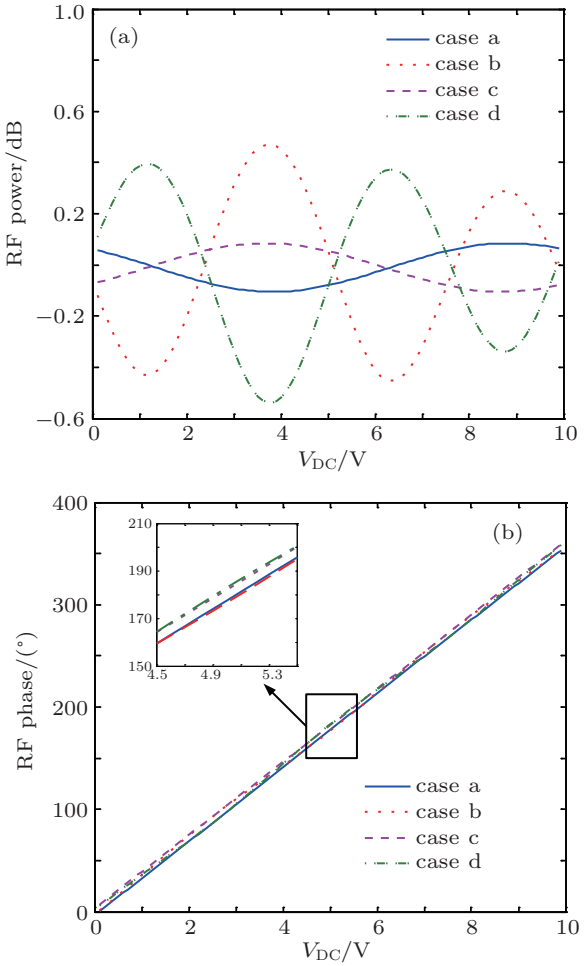


Fig. 4. (color online) (a) Calculated RF power (normalized by P_Ω in Eq. (15)) as a function of DC voltage; (b) Calculated RF phase as a function of DC voltage. Case (a): (3%, 3%); case (b): (−3%, 3%); case (c): (−3% −3%); case (d): (3%, −3%). The half-switching voltage is $V_\pi = 5$ V, the modulation index is fixed at $m = 1$.

To further show the impact of bias drift on the proposed RF phase shifter, the RF power and phase characteristic maps are shown in Figs. 4(a) and 4(b) with the bias conditions of (ΔV_1, ΔV_2): case (a): (3%, 3%); case (b): (−3%, 3%); case (c): (−3%, −3%); and case (d): (3%, −3%), respectively. The RF power is normalized by P_Ω in Eq. (15). Half-wave switching voltage is set as $V_\pi = 5$ V, and modulation index at $m = 1$. As shown in Fig. 4(a), the power variation is pretty small (peak to peak magnitude less than 1 dB), which agrees well with the results in Figs. 2(a), 2(b), 2(c), and Fig. 3. Then figure 4(b) shows the RF phase characteristics. Note that all lines are overlapped with each other. Even zooming in (inserted), the difference is negligible. We can set the modulation index m to other values, e.g., $m = 1.5$, 2, 2.5, but the results will not change much. It is concluded that very stable performance can be guaranteed under the condition that the bias drift is within the range of −3%∼ 3%.

4. Verification by simulation

In the above analysis, the coupling ratios of two MMI are considered as perfectly 50:50. In practice, it cannot be satisfied. Thus it is necessary to discuss this issue and also verify the proposal. In this section, a proof-of-concept simulation is conducted via Opt-System 10.0. The key components, the 1×2 MMI and the 1×4 MMI, are designed by a Matlab program. As shown in Fig. 5, a light from a CW laser source at wavelength of $\lambda_0 = 1550$ nm with a linewidth of 800 kHz is coupled to the 1×2 MMI. In the figure, $\gamma_1 = 45\%$ and $\gamma_2 = 55\%$ represent the power splitting coefficient of MMI, thus the coupling ratio of MMI used in the simulation is 45:55. Then the 1×4 MMI is connected. To simplify the verification, the 1×4 MMI is designed by integration of three 1×2 MMIs. Thus the 1×4 MMI's power splitting coefficient is set as $\gamma_1\gamma_2$, γ_{12}, $\gamma_2\gamma_1$, and γ_{22}, which are proportional to that

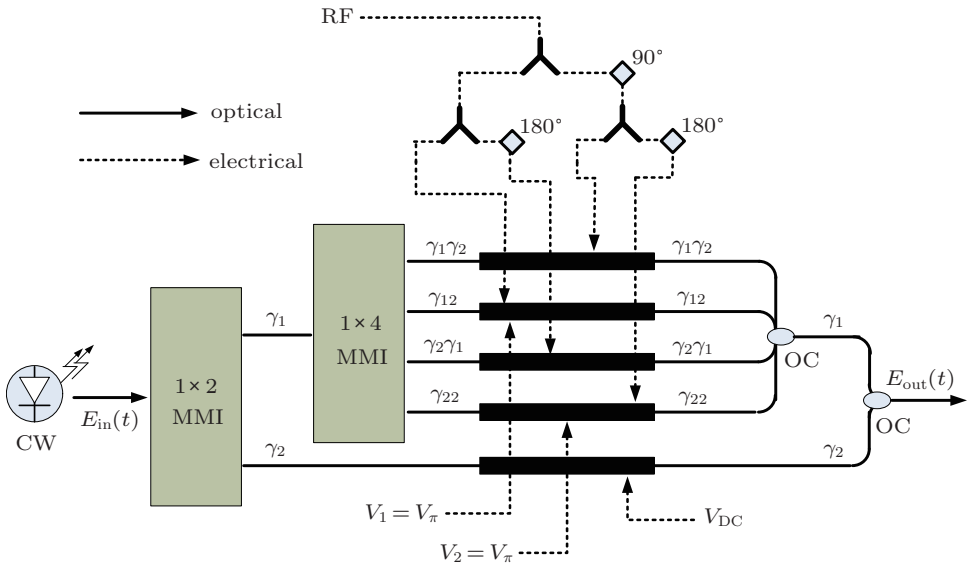


Fig. 5. (color online) Simulation setup of the proposal.

of the 1×2 MMI. The phase modulation is implemented by using five phase modulator. The upper four are driving with 30-GHz RF signal. Under small signal modulation (modulation index $m = 1$), lightwaves are coupled into a 4×1 OC, whose coupling ratio is the same with the 1×4 MMI. At the output of the 4×1 OC, optical spectrum can be obtained as shown in Fig. 6(a). The number in the figure indicates the order of sidebands. It is seen that the carrier and −1st order sideband are suppressed thus SSB-CS (single sideband with carrier-suppression) is obtained. Also note that due to the MMI's improper coupling ratio (45:55), the carrier and ±2nd order sidebands are not fully suppressed, which will introduce distortion to the RF power and phase. The carrier-to-sideband ratio (CSR) is −23 dB. Theoretically, the beating of carrier to 1st, 1st to 2nd, and −3rd to −2nd order harmonics will generate RF signal at a frequency of 30 GHz, but with no phase shifting. Then a 2×1 OC is used to combine lightwaves from the upper four arms and the fifth arm with DC control. The DC voltage controlled phase shifting is φ_3. Then the output spectrum is shown in Fig. 6(b). The CSR becomes 7 dB. Due to the small signal modulation, the impact of high order harmonic (±2nd and −3rd) is very small. Afterwards, $E_{\text{out}}(t)$ can be detected by a photodiode. The temporal waveform and RF power can be obtained.

Increasing φ_3 from 0° to 360°, figure 7 shows the evolution of temporal waveform at different φ_3. As shown in Fig. 7, very good waveform is achieved and no significant phase mismatch is observed. Then figure 8 shows the simulated RF power as a function of φ_3. Compared with the results in Fig. 4(a), the impact of MMI's improper coupling ratio (45:55) is shown in circle (i.e. no bias drift). Apparently, the impact is very small, peak-to-peak magnitude around 0.5 dB. Except for the no bias drift condition, other four lines in Fig. 8 represent four different bias conditions in (ΔV_1, ΔV_2): case (a): (3%, 3%); case (b): (−3%, 3%); case (c): (−3%−−3%); and case (d): (3%, −3%). To some extent, simulated results in Figs. 8 and 7 agree with the calculated results in Figs. 4(a) and 4(b). It can be seen that the combination impact of MMI's improper coupling ratio and bias drift is still small. Therefore, a bias drift range should be within −3% and 3%. With the help of active bias control, such a range can be easily achieved in practice and steady performance can be guaranteed. Furthermore, because the RF signal power variation and phase accuracy are hardly dependent on modulation index, RF signal power can be increased by simply tuning the modulation index. This is an additional advantage when compared to Refs. [5] and [6].

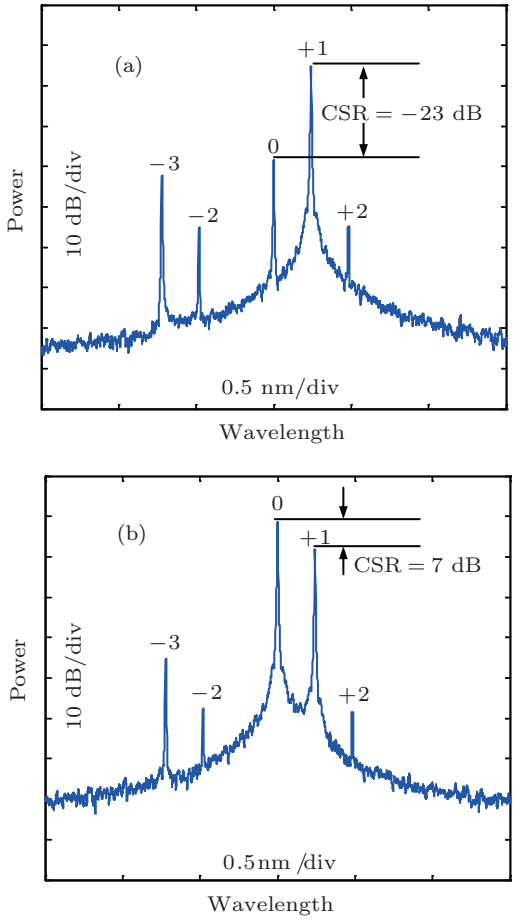


Fig. 6. (color online) Simulated optical spectra at the output of (a) 4×1 OC and (b) 2×1 OC.

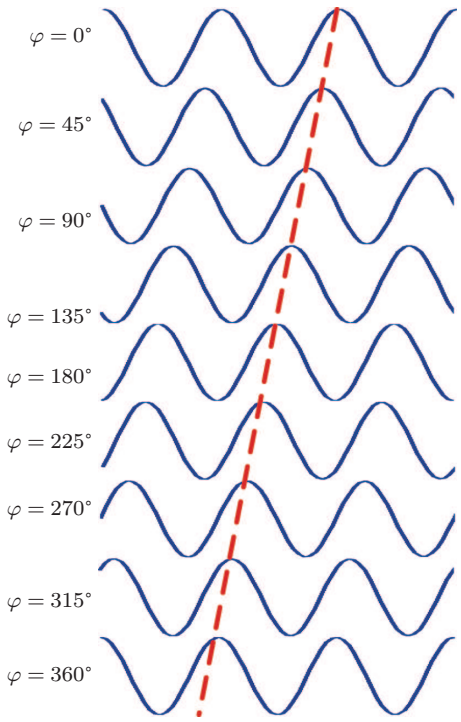


Fig. 7. (color online) Simulated evolution of temporal waveform (no bias drift) at different φ_3 (0° ∼ 360°), the red line marks the reference point of waveforms.

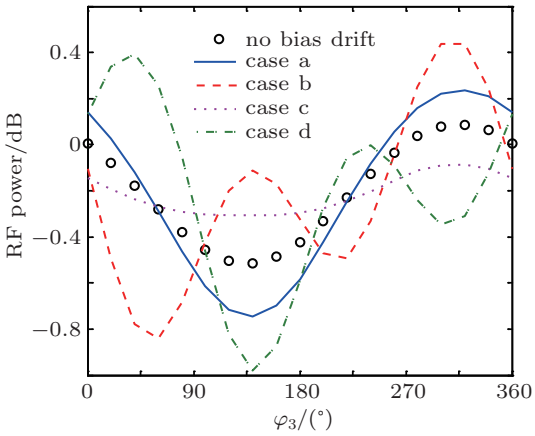


Fig. 8. (color online) Simulated RF power (normalized) as a function of DC voltage controlled phase shift φ_3. Five different bias conditions are included: with no bias drift, cases a, b, c, and d.

5. Conclusion

A photonic approach for RF phase shifting with DC voltage control is proposed and verified by theory and simulation. The proposed RF phase shifter can be realized using a polymer-based integrated Mach–Zehnder modulator (IMZM). Both analysis and simulation are carried out to investigate the performance of this phase shifter. It is found that phase shifting with an RF signal power variation lower than 1 dB and phase accuracy less than 3° can be achieved if two MZM bias voltage drifts are within −3%∼3%. It is also found that the RF phase shifter is a little degraded by perturbation of modulation index, i.e., RF signal power variation and phase accuracy are almost immune to perturbation of modulation index. A proof-of-concept simulation is carried out to verify its principle. Besides, the impact of MMI's improper coupling ratio (45:55) has been discussed and proved to be small. However, in the present prototype, the frequency coverage may be enhanced by using polymer optical–electrical modulators but is still dependent on three RF hybrid couplers which are also bandwidth-limited. Thus there is still room for improvement. For example, the stimulated Brillouin scattering-based microwave signal processing technique[22–24] can be employed to simplify the prototype, since it has the advantage of single-pass configuration, not multiple-parallel pass configuration.

References

[1] Xu E M, Zhang X L, Zhou L N, Zhang Y and Huang D X 2009 *Chin. Phys. Lett.* **26** 94208
[2] Dong J J, Luo B W, Yu Y and Zhang X L 2012 *Chin. Phys. B* **21** 068401
[3] Li R G, Jiang S W, Gao L B and Li Y R 2013 *Chin. Phys. Lett.* **30** 078503
[4] Huang J, Zhao Q, Yang H, Dong J R and Zhang H Y 2013 *Chin. Phys. B* **22** 127307
[5] Lee S S, Udupa A H, Erlig H, Zhang H, Chang Y, Zhang C, Chang D H, Bhattacharya D, Tsap B, Steier W H, Dalton L R and Fetterman H R 1999 *IEEE Microwave and Guided Wave Lett.* **9** 357
[6] Han J, Seo B J, Kim S K, Zhang H and Fetterman H R 2003 *J. Lightwave Technol.* **21** 3257
[7] Coward J F, Chalfant C H and Chang P H 1993 *J. Lightwave Technol.* **11** 2201
[8] Chan E H W and Minasian R A 2006 *J. Lightwave Technol.* **24** 2676
[9] Fisher M R and Chuang S L 2006 *IEEE Photon. Technol. Lett.* **18** 1714
[10] Loayssa A and Lahoz F J 2006 *IEEE Photon. Technol. Lett.* **18** 208
[11] Han J, Erlig H, Chang D, Oh M C, Zhang H, Zhang C, Steier W and Fetterman H 2002 *IEEE Photon. Technol. Lett.* **14** 531
[12] Chang Q J, Li Q, Zhang Y H, Qiu M, Ye T and Su Y K 2009 *IEEE Photon. Technol. Lett.* **21** 60
[13] Xue W Q, Sales S, Capmany J and Mørk J 2010 *Opt. Express* **18** 6156
[14] Sancho J, Lloret J, Gasulla I, Sales S and Capmany J 2011 *Opt. Express* **19** 17421
[15] Jez D R, Cearns K J and Jessop P E 1997 *Microwave Opt. Technol. Lett.* **15** 46
[16] Rahman B M A, Haxha V, Haxha S and Grattan K T V 2006 *J. Lightwave Technol.* **24** 3506
[17] Song R, Song H C, Steier W H and Cox C H 2007 *IEEE J. Quantum Electron.* **43** 633
[18] Chen D T, Harold R F, Chen A T, William H S, Larry R D, Wang W S and Shi Y Q 1997 *Appl. Phys. Lett.* **70** 3335
[19] Blahut M and Optilski A 2001 *Opt. Electron. Rev.* **9** 293
[20] Pei L, Liu G H, Ning T G, Gao S, Li J and Zhang Y J 2012 *Acta Phys. Sin.* **61** 064203 (in Chinese)
[21] Li J, Ning T G, Pei L, Jian W, You H D, Chen H Y, Zhang C and Li C 2013 *Acta Phys. Sin.* **62** 224210 (in Chinese)
[22] Li W, Zhu N H, Wang L X and Wang H 2011 *J. Lightwave Technol.* **29** 3616
[23] Byrnes A, Pant R, Li E B, Choi D Y, Poulton C G, Fan S H, Madden S, Luther-Davies B and Eggleton B J 2012 *Opt. Express* **20** 18845
[24] Zou X H, Li W Z, Pan W, Yan L S and Yao J P 2013 *IEEE Trans. Microwave Theor. Techniq.* **61** 3470